Can Metallic Sodium Electrodes Affect the Electrochemistry of Sodium-Ion Batteries? Reactivity Issues and Perspectives

Kristina Pfeifer,[a] Stefanie Arnold,[a] Julian Becherer,[a] Chittaranjan Das,[a] Julia Maibach,[a] Helmut Ehrenberg,[a, b] and Sonia Dsoke*[a, b]

Sodium-ion batteries (NIBs) are promising energy-storage devices with advantages such as low cost and highly abundant raw materials. To probe the electrochemical properties of NIBs, sodium metal is most frequently applied as the reference and/or counter electrode in state-of-the-art literature. However, the high reactivity of the sodium metal and its impact on the electrochemical performance is usually neglected. In this study, it is shown that spontaneous reactions of sodium metal with organic electrolytes and the importance of critical interpretation of electrochemical experiments is emphasized. When using sodium-metal half-cells, decomposition products contaminate the electrolyte during the electrochemical measurement and can easily lead to wrong conclusions about the stability of the active materials. The cycling stability is highly affected by these electrolyte contaminations, which is proven by comparing sodium-metal-free cell with sodium-metal-containing cells. Interestingly, a more stable cycling performance of the $Li_4Ti_5O_{12}$ half-cells can be observed when replacing the Na metal counter and reference electrodes with activated carbon electrodes. This difference is attributed to the altered properties of the electrolyte as a result of contamination and to different surface chemistries.

Introduction

Enormous interest in post-lithium energy-storage systems has developed over the past several years.[1] As lithium-ion batteries (LIBs) are the major power sources for electrical vehicles and portable electronic devices, the demand on available lithium resources is rapidly increasing.[2] However, by exploiting lithium sources for these purposes, the price of the metal will dramatically rise as a consequence of the growing electrification.[3] A promising alternative technology is the sodium-ion battery (NIB), which provides the advantages of highly abundant sodium, low cost, and a similar intercalation chemistry to that of lithium.[4,5] Various combinations of organic electrolytes and materials known from LIB technology have shown promising results for NIBs.[5–10] Therefore, a wide range of experiments have been transferred from LIB systems to NIB systems in the state-of-the-art literature. Nevertheless, the increased reactivity of sodium metal, which is used as a counter and reference electrode for electrochemical half-cell tests, usually remains neglected. Iermakova et al.[11] discovered a reduced electrochemical stability of symmetric Na/Na cells in conventional organic electrolytes compared with Li/Li cells. They presumed effects like electrolyte decomposition and electrical contact loss between metallic Na and the current collector as the main root cause for this behavior.[11] Likewise, Zarrabeitia et al.[12] observed an influence of the sodium metal when comparing $Na_2Ti_3O_7/NaFePO_4$ full-cells with $Na_2Ti_3O_7/Na$ half-cells. Additionally, Conder and Villevieille[13] showed that achieving passivation of the sodium surface is hardly manageable in electrochemical cells. They proposed an optimized fabrication of sodium metal electrodes with attention to a smooth and clean surface and the thickness of the metal.
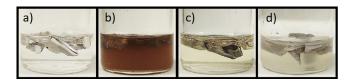
Using Na metal as the counter and/or reference electrode leads to a detrimental distortion of the electrochemical measurement (e.g., the active material under investigation). In this work, we present novel insights into the reaction processes of sodium metal towards organic carbonate electrolytes. For this purpose, we compare the established Na half-cell with activated carbon (AC) counter and quasi-reference electrodes (QREs). Such QREs have been reported as suitable alternative reference electrodes in several electrochemical systems.[14] Additionally, AC has been successfully used as a counter electrode, showing a stable behavior, which is influenced by different surface groups.[15–17] We underline the importance for critical reflection of data gained from electrochemical experiments concerning the application of cell setups for NIBs.

[a] K. Pfeifer, S. Arnold, J. Becherer, Dr. C. Das, Dr. J. Maibach,
Prof. H. Ehrenberg, Dr. S. Dsoke
Institute for Applied Materials (IAM)
Karlsruhe Institute of Technology (KIT)
Hermann-von-Helmholtz-Platz 1, 76344 Eggenstein-Leopoldshafen (Germany)
E-mail: sonia.dsoke@kit.edu

[b] Prof. H. Ehrenberg, Dr. S. Dsoke
Helmholtz-Institute Ulm for Electrochemical Energy Storage (HIU)
P.O. Box 3640, 76021 Karlsruhe (Germany)

The ORCID identification number(s) for the author(s) of this article can be found under:
https://doi.org/10.1002/cssc.201901056.

Results and Discussion

Reactivity of sodium towards organic electrolytes

Sodium metal was reported to have an influence on the electrochemical performance of half-cells during cycling.[11,12] Typically, organic carbonates such as ethylene carbonate (EC), dimethyl carbonate (DMC), diethyl carbonate (DEC), propylene carbonate (PC), etc. are the most frequently used solvents for Na salts like sodium perchlorate ($NaClO_4$) or sodium hexafluorophosphate ($NaPF_6$) to form the commonly used electrolytes.[7,18,19] By placing Na metal inside such electrolytes, as shown in Figure 1, we were able to visualize clearly that
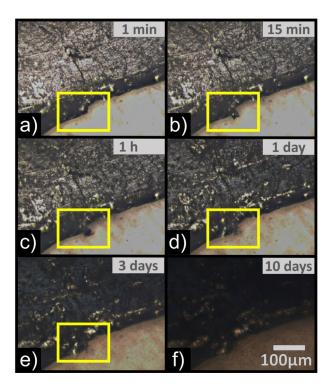

Figure 1. a) Na metal in E-$NaClO_4$ right after Na addition (representative for all electrolytes). b) Na metal in E-$NaClO_4$, c) in P-$NaClO_4$, and d) in E-$NaPF_6$ after three days.

sodium reacts with the different electrolytes, even without electrochemical cycling. The electrolytes will be referred as E-$NaClO_4$ (1 M $NaClO_4$ in EC/DMC), E-$NaPF_6$ (1 M $NaPF_6$ in EC/DMC), and P-$NaClO_4$ (1 M $NaClO_4$ in PC). A more detailed description is given in the Experimental Section. Immediately after Na addition, the metal exhibits a shiny metallic surface and the liquid electrolytes are colorless and clear in all cases (see Figure 1 a). After three days, a difference appears between the different electrolytes. A massive color change can be observed for E-$NaClO_4$ in Figure 1 b. The clear solution turns to dark red and turbid after three days. Also, in case of E-$NaPF_6$ (see Figure 1 d), the solution turns cloudy but remains colorless. In the case of P-$NaClO_4$, shown in Figure 1 c, the solution turns slightly yellow but remains clear. These changes are likely caused by side reactions with the electrolyte. The surface of the Na metal has altered in all three samples. From this simple optical examination, it is possible to conclude that spontaneous reactions take place in all electrolytes and that sodium forms decomposition products with the electrolyte.

To obtain a deeper understanding of the processes occurring on the sodium surface, optical micrcopy was conducted over the timeframe of the experiment. A sealed microscopy cell with Na metal on a polyethylene (PE) film and filled with E-$NaClO_4$ was prepared. To monitor the changes on the metal surface, boundary, and the PE film, an area at the edge of the Na metal was chosen for the observation (Figure 2). The transformation process over 10 days is visualized in Figure 2 a–f. An outgrowth is formed after only 15 min as can be seen when comparing the highlighted area in Figure 2 a and b. With increasing time, this particle shrinks again (highlighted section in Figure 2 d). Finally, it entirely vanished after three days (Figure 2 e). According to this study, a conversion of the Na metal surface over time becomes evident. The shiny and smooth Na-

Figure 2. Optical microscopy images of Na metal on a polyethylene film, filled with E-$NaClO_4$ in a sealed sell. Pictures were recorded after a) 1 min, b) 15 min, c) 1 h, d) 1 d, e) 3 d, and f) 10 d. The yellow highlighted area shows a time-resolved reaction on the Na surface.

metal surface in Figure 2 a turns dark and becomes rougher (see Figure 2 c–f). We relate these observations to the formation of a solid interphase consisting of degradation products of reactions between Na and the electrolyte. However, particles of this phase are continuously peeled off and diffuse into the electrolyte. Afterwards, the blank Na surface can further react with the electrolyte. This assumption is supported by the turbid appearance of E-$NaClO_4$ and E-$NaPF_6$ (Figure 1) and the decrease of the image intensity during optical microscopy (Figure 2 c–f). Both effects are likely caused by the interaction of light with the particles in the electrolyte. As PE does not react with the electrolyte, the reduced intensity must be caused by a cloudier electrolyte and the image cannot just become darker as a result of the rougher surface or color change.

These findings raise serious doubts about the use of Na metal for electrochemical investigations. Indeed, even without electrochemical cycling, high reactivity of the sodium metal is demonstrated (Figures 1 and 2). Decomposed species can diffuse inside the electrolyte and can thus interact with the electrochemical system under investigation. Not only instabilities of the passivation layer but also dendrite-like changes of the Na surface can lead to short circuits in the cell. Moreover, the side reactions taking place at the Na/electrolyte surface are possibly amplified during electrochemical cycling (i.e., when using the Na metal as a counter electrode). Such effects likely result in distorted conclusions about the tested materials. However, the three-electrode setup is still indispensable for the investigation of the behavior of single electrodes.[20] Sensitive techniques like electrochemical impedance spectroscopy

require a reliable reference electrode (RE) with a stable potential over time.[21] A reactive Na metal RE cannot guarantee this as polarization effects cannot be excluded. Consequently, there is not only a lack of reliability for the described half-cell measurements, but also transfer of the results to a full cell would not be consistent as already observed in Ref. [12].
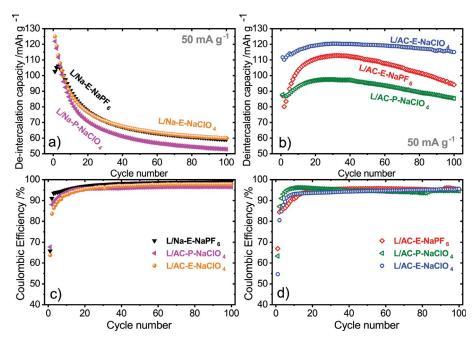
Influence of metallic sodium in electrochemical cells

To study the impact of Na metal in an electrochemical cell, the reactivity of Na metal towards the electrolyte during cycling has to be considered. Comparing symmetric hard carbon cells with three-electrode cells consisting of a Na counter and reference electrode and a hard carbon working electrode, an unstable behavior of the solid electrolyte interphase (SEI) owing to decomposition products was assumed by Iermakova et al.[11] For such an analysis, materials like hard carbon are not optimal as they show a very low intercalation profile below 0.1 V (vs. Na/Na+).[22,23] This potential is below the stability window of organic electrolytes and may cause sodium plating and stripping on the electrode surface.[22,23] Consequently, it cannot be distinguished between degradation products, which occur as a result of reactions with Na, and the ones that can form owing to electrolyte decomposition at low potential. Additionally, sodium plating and stripping may change the surface and the SEI and can cause additional reactions between the electrolyte and the plated sodium metal.

We selected $Li_4Ti_5O_{12}$ (LTO) as a suitable reference material to evaluate the impact of Na metal on the electrolyte. LTO possesses a higher intercalation potential at about 0.9 V (vs. Na/Na+) and a high stability during cycling.[9,19] Furthermore, the intercalation mechanism of Na ions into LTO is well investigated in terms of the change of the crystal structure during cycling.[8,19,24,25]

For this reason, in this work, LTO was employed as exemplary working electrode material in two different cell setups: one using Na metal as the counter and reference electrode, one using activated carbon (AC) as the counter and reference electrode. All electrochemical measurements were conducted by using a three-electrode configuration. The cell-setup labelling will from hereon be L/Na and L/AC, respectively. Figure 3 a and b demonstrate the difference in cycling stability, comparing both setups and using three different electrolytes. All L/Na cells show a rapid capacity loss of more than 35% during the initial 20 cycles (Figure 3 a). The capacity gradually stabilizes, but a continuous decrease can be observed during further cycling. Starting with initial capacities of 105–125 mAh g^{-1}, the L/Na cells end up below 60 mAh g^{-1} after 100 cycles, which is a loss of about 40–55%. On the contrary, the L/AC cells first show an increase in capacity during the initial 20 cycles, followed by a stabilization period (Figure 3 b). After 100 cycles, the capacity retention for these cells is more than 83% of their maximum capacity. In fact, the L/AC-E-NaClO$_4$ shows the highest capacity during cycling, combined with the most stable behavior, exhibiting 96% of its maximum capacity after 100 cycles. These results contradict the conclusions of Sun et al.[19] and Zhao et al.;[26] both solely related the rapid capacity loss of similarly composited LTO working electrodes to the reactivity of the used polyvinylidene fluoride (PVdF) binder. Their measurements were conducted with Na metal counter and reference electrodes. Our results can confirm the unstable cycling behavior of LTO in a Na half-cell setup and clearly show more stable performance when no Na metal is present in the electrochemical setup.

By further comparing L/Na with L/AC cells, additional insights can be gained. In general, the L/AC cells exhibit strong capacity differences when comparing the different electrolytes. Thus, without Na metal contact, the different electrolyte prop-

Figure 3. Comparison of L/Na and L/AC cell performance with different organic electrolytes at charging/discharging currents of 50 mA g^{-1}. a) Electrochemical cycling stability of L/Na cells. b) Electrochemical cycling stability of L/AC cells. c) Coulombic efficiencies of L/Na cells. d) Coulombic efficiencies of L/AC cells.

erties become apparent. We relate the distinctions of the L/AC cells to electrolyte properties such as conductivity, viscosity, dielectric constants, or differences in the formed SEI.[5] For cells containing sodium metal, these small electrochemical nuances cannot be illuminated owing to the impact caused by the electrolyte contaminations. Additionally, the properties of the electrolyte in Na-containing half-cells could have changed as a result of the degradation products. The initial capacity increase of the L/AC cells is related to the known conditioning process during the first cycles, which facilities further sodiation reactions.[8, 9] This effect is not visible for L/Na cells, which could be related to the contaminated electrolyte. We cannot give an explicit functional mechanism in the current study, as this would require knowledge of detailed processes that are taking place in narrow atomic dimensions close to the counter electrode/electrolyte interface.

The coulombic efficiencies (CEs) are given in Figure 3 c, d to evaluate the disparities between both cell setups. All cells start with CEs below 70%, reaching 90% after ten cycles. Such behavior is attributed to the rearrangement of the LTO crystal structure[9, 27] and to side reactions of the cell components, leading to SEI formation.[28] In general, the CEs of all cells are relatively similar. L/Na cells reach CEs of more than 96% (Figure 3 c) whereas L/AC cells reach 93–95% (Figure 3 d). Considering the lower CE of the L/AC cells, the reactivity of the electrolytes towards the AC surface groups should be taken in account. Such surface characteristics of AC counter electrodes might lead to side reactions between the AC surface groups and the electrolyte or undesirable polarization effects.[15, 16, 29] Therefore, we want to highlight that the chosen AC setup is not the optimal alternative to the established Na metal setup. Nonetheless, we observe explicit differences when comparing the electrochemical performance of both setups. Hence, the reactivity of Na metal towards the electrolyte affects the electrochemical system to a greater extent than when using the AC setup. Further work is required to uncover the underlying processes of the low CE to further improve the electrochemical properties.

In the following, we will demonstrate the impact of degraded species on the working electrode bulk material by ex situ XRD analysis and on the electrode surface chemistry by X-ray photoelectron spectroscopy (XPS) analysis.

Impact of Na metal reactivity on the bulk material after electrochemical cycling

The electrochemical properties of LTO have been well investigated for Li-ion insertion/extraction[8, 24, 30] as well as for Na-ion intercalation/deintercalation.[8, 9, 19, 25, 31] In the case of Na ions, Sun et al.[19] predicted a three-phase storage mechanism, $2Li_4Ti_5O_{12} + 6Na^+ + 6e^- \rightleftharpoons Li_7Ti_5O_{12} + Na_6LiTi_5O_{12}$, and proved it by in situ X-ray diffraction measurements. Additionally, Yu et al.[25] confirmed these findings. Figure 4 a and b illustrates the galvanostatic charge/discharge profiles of the second and 50th cycles for L/Na-E-NaClO₄ and L/AC-E-NaClO₄, respectively. Comparing the sodiation curves of the second and 50th cycles, a difference is evident between 1.2 and 0.9 V (vs. Na/Na⁺; Fig-
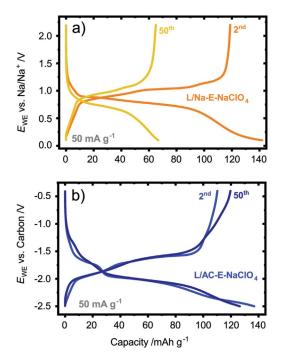

Figure 4. Galvanostatic charge and discharge profiles of the second and 50th cycle for a) L/Na-E-NaClO₄ and b) L/AC-E-NaClO₄.

ure 4 a) and between −1.3 and −1.6 V (vs. carbon; Figure 4 b). This can be attributed to structural rearrangements during the initial cycling. Nevertheless, the first sodiation plateau of cycle 50 at −1.6 V (vs. carbon) is significantly pronounced (Figure 4 b). At the same time, this plateau is not apparent for the L/Na-E-NaClO₄ cell. As a three-phase mechanism can be indicated by multiple plateaus, we assume that decomposition products result in hindered Na-ion insertion/extraction, causing lower capacities.

To examine if decomposed species have an influence on the active bulk of LTO, we performed XRD measurements of the cycled electrodes. For this purpose, L/Na-E-NaClO₄ and the respective L/AC-E-NaClO₄ electrode materials were measured by XRD in the desodiated state after 100 cycles and compared with pristine LTO (Figure 5). Even though the cells were desodiated by a subsequent voltage hold after discharging, a small amount of a residual Na-containing phase remained. The diffractograms of cycled LTO both verify the formation of a sodiated structure, indicated by shoulders that are located below the 111, 311, and 400 reflections of LTO.[19] Moreover, the reflections of the Li₄Ti₅O₁₂/Li₇Ti₅O₁₂ phase can be identified (ICSD #182954). The identical shape of both cycled materials proves that contaminations, which originate from reactions between Na and the electrolyte, do not change the bulk material. Indeed, the structural properties of LTO after cycling are identical for both cell setups. Therefore, it seems that solely the surface of the working electrode is affected by side reactions with decomposed electrolyte species and will be analyzed in the following.
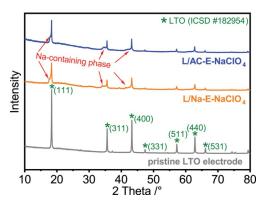
Figure 5. XRD patterns of cycled L/AC-E-NaClO$_4$ and L/Na-E-NaClO$_4$ electrodes and the respective pristine LTO electrode.

Surface analysis after electrochemical cycling

To understand the chemistry of the surface and its correlation with the performance and stability, XPS measurements were conducted on the LTO electrodes of both setups for three different electrolytes. All spectra are corrected with respect to the peak position at 285.0 eV (—CH$_2$—)[32,33] from the pristine LTO electrode sample. The F 1s core level in Figure 6a shows that the pristine LTO has a single peak at 688.0 eV, which corresponds to the —CF$_2$— groups from the PVdF binder.[33,34] When the LTO electrodes are sodiated, two peaks appear. The signal at 684.0 eV can be assigned to LiF and NaF;[35,36] for all samples, these peaks appear at similar binding energies. In contrast, the second peak is shifted when comparing the spectra with regard to the different cell setups. In the case of the AC samples, the second signal appears at 687.8 eV whereas for the samples cycled versus Na, it is shifted to 687.0 eV and indicated by "#" in Figure 6a. As previously reported by Dahbi et al.,[36] this shift is assigned to a decomposition of the PVdF

binder owing to defluorination. Consequently, if Na metal is used as counter and reference electrode, the decomposition of PVdF is more severe and can affect the cycling stability of the working electrode.

Considering the C 1s spectra (Figure 6b), the pristine LTO electrode shows an intense peak at 284.2 eV corresponding to the graphitic parts of the conductive additive. Additionally, there are other peaks at 285.0, 286.3, 288.7, and 291.0 eV, which are assigned to —CH$_2$—, —CF$_2$—C*H$_2$—, O=C—O, and —C*F$_2$—CH$_2$—+CO$_3$—, respectively.[32–34,37] When comparing the spectra with regard to solely the setup properties, the sodiated electrodes show very similar spectra for all AC setups. The same is observed for the Na setup, independently of the electrolyte. This indicates that the surface layers that form on the LTO electrodes depend more on the type of counter electrode than on the type of electrolyte used. Moreover, the C 1s and F 1s spectra for all AC samples have a lower intensity than that of the Na samples (Figure 6 a, b). This indicates that the surface layer appears to be thicker for all AC samples than the Na samples. The most prominent difference in the C 1s spectra appears in the region between 289 eV and 291 eV. Two signals are observed for the AC samples at 289.3 eV and 290.7 eV whereas only one is present for all Na samples at 290.0 eV and is marked with "#" in Figure 6b. For the AC samples, the peak at the higher binding energy is assigned to the PVdF binder and possibly to organic carbonates. The new signal at around 289.3 eV is most likely due to Na$_2$CO$_3$ or alkyl carbonates R-OCO$_2$Na.[32,33] At 290.0 eV, a signal appears only for the Na samples and cannot be identified. Still, it could be related to PVdF decomposition as there is no clear signal in the CF$_2$ region anymore. This assumption fits well with the shifted F 1s peak at 687.0 eV (Figure 6a). Therefore, in the case of the Na samples, the binder seems to be more affected by the decomposed electrolyte owing to the presence of Na in the half-cell. In gen-
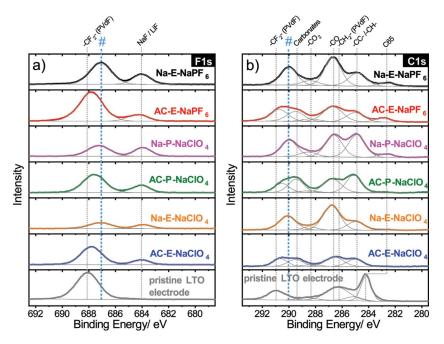

Figure 6. a) F 1s and b) C 1s spectra of the pristine LTO electrode and all samples after 20 cycles in the sodiated state with proposed assignments.

eral, decomposition products do not only lead to altered electrolyte properties but also affect the working electrode surface, which can impair the electrochemical stability.

Conclusions

The reactivity of sodium metal towards the electrolyte was evaluated by microscopic and macroscopic optical observation. It was shown that a decomposition of the sodium surface and the electrolyte takes place very rapidly even without electrochemical cycling. To analyze such decomposition effects on the electrochemical performance, the commonly used Na half-cell setup was compared with a sodium-metal-free half-cell. It was possible to prove that a significant difference in the electrochemical stability appears when comparing sodium-containing half-cells to sodium-free ones. When sodium was used as the counter and reference electrode, a fast decrease of the $Li_4Ti_5O_{12}$ (LTO electrode capacity was determined. A different behavior for the same working electrode was discovered after replacing sodium electrodes with activated carbon (AC) electrodes. We expect that the side reactions between sodium and the electrolytes are enhanced by electrochemical cycling experiments. This drastically impairs the stability of sodium half-cells. Additionally, ex situ XRD analysis showed that decomposition products do not influence the crystal structure of the active material. XPS measurements were conducted to demonstrate that the occurring instabilities are caused by electrolyte contaminations and to evaluate their impact on the surface chemistry. Such distortions could lead to wrong conclusions of electrochemical experiments and problems in transferring half-cell results to full cells. Additional work should focus on improving alternative counter and reference electrodes, as avoiding sodium seems to be essential for reliable electrochemistry. Attention should be payed especially to the influence of surface species on AC electrodes. It is also important to find an alternative Na source in the counter electrode to avoid the consumption of Na^+ ions from the electrolyte.

Experimental Section

Electrolytes

The preparation and handling of the electrolyte solvents and salts was conducted in an argon-filled glovebox (MBraun, O_2 and H_2O < 0.5 ppm). All sodium salts were dried under vacuum at 80 °C for 48 h. Three different combinations of organic solvents and sodium salts were prepared: 1 M sodium perchlorate (NaClO₄, Alfa Aesar, > 99%) was dissolved in propylene carbonate (PC, Sigma–Aldrich, 99.7%) and in a mixture of 1:1 (by mass) ethylene carbonate (EC, Sigma–Aldrich, ≥ 99%) and dimethyl carbonate (DMC, Sigma–Aldrich, ≥ 99%). Additionally, 1 M sodium hexafluorophosphate (NaPF₆, Alfa Aesar, > 99%) was dissolved in a 1:1 (by mass) mixture of EC and DMC. All prepared electrolytes were examined by Karl–Fischer titration and were found to contain less than 25 ppm water. The electrolytes are labeled as E-NaClO₄ (1 M NaClO₄ in EC/DMC), E-NaPF₆ (1 M NaPF₆ in EC/DMC), and P-NaClO₄ (1 M NaClO₄ in PC).

Optical characterization

For visual analysis of the Na reactivity, Na metal pieces (0.25 g, Alfa Aesar, 99.95%) were thoroughly cleaned by scraping the surface layer of the metal with a scalpel in an argon-filled glovebox to remove any impurities on the metal surface. These shiny metal pieces were added to 5 mL of each of the three different electrolytes. Pictures were taken right after the addition of the metal and three days later.

For optical microscopy studies, the microscopy cell consisted of a polyethylene (PE) film, an O-ring, and a borosilicate glass, which were clamped between two metal plates to seal the cell. The upper metal plate was perforated to enable optical microscopy through the underlying borosilicate window. The sodium metal was pressed onto the polyethylene film and the cell was filled with the electrolyte (1 M NaClO₄ in EC/DMC) inside an argon-filled glovebox. Bright field imaging with an Olympus BXFM microscope at 10× magnification was performed. To increase the depth of field, focus stacks consisting of 25 single CCD images with 8 μm distance between the focal planes were taken. During the experiment, images were recorded every 15 min.

Electrode materials and preparation

Activated carbon (AC) powder was obtained from HayCarb PLC and conductive additive powder carbon black (CB) type C-NERGY C65 from Imerys Graphite & Carbon. Nanometer-sized lithium titanate (LTO, type: lithium titanate, spinel, nanopowder) was purchased from Sigma–Aldrich.

Working electrodes were prepared by mixing 80 mass% LTO powder with 10 mass% CB and 10 mass% polyvinylidene fluoride (PVdF) dissolved in dimethyl sulfoxide (DMSO) in a DAC150.1 FVZ speed-mixer from Hauschild. LTO and CB were first dry mixed at 1000 rpm for 5 min. Then, DMSO was added to obtain a viscous paste. This paste was again mixed at 1500 rpm for 10 min, followed by 2500 rpm for 10 min, before adding the binder solution. The last mixing step was conducted at 800 rpm for 10 min. PVdF was used as the binder for the LTO working electrodes as it is one of the most frequently used binders in LIBs as well as in NIBs.[7,8,10] The slurries were doctor bladed onto an aluminium foil and dried for three days at ambient conditions. Subsequently, the electrodes were punched out (12 mm in diameter) and transferred into a vacuum oven inside an Ar-filled glovebox. Finally, a vacuum drying step at 120 °C for 12 h was conducted. The thickness of the dried LTO electrodes was typically 25 μm with a mass loading of 3 ± 1 mg cm^{-2} (the full electrode mass including the current collector was 8 ± 1 mg cm^{-2}).

For the preparation of the counter and QRE, AC was mixed with isopropanol in a DAC150.1 FVZ speed mixer. For the transformation to a paste, 10 mass% (dry mass) of dissolved polytetrafluoroethylene (PTFE, 60 mass% solution in water from Sigma–Aldrich) was added to the mixture and speed-mixed at 800 rpm for 5 min. The utilization of PTFE binder has the advantage of obtaining a highly oversized AC electrode to avoiding electrode cracking. To obtain a viscous consistency, the paste was kneaded manually on a glass plate. It was then placed between two PE foils and manually rolled to a thickness of 1 ± 0.25 mm. Discs with 12 mm diameter were punched out after drying for 12 h in ambient atmosphere. The mass of the counter electrode was typically 100 ± 5 mg cm^{-2}. The remaining parts were kept and used as the QRE. The electrodes were transferred to a vacuum oven inside an Ar-filled glovebox and dried at 120 °C for 24 h under vacuum. The initial potential difference between the used HayCarb AC QRE and metallic sodium was determined to be 2.6 V.

Cell preparation and electrochemical characterization

Custom-built polyether ether ketone (PEEK) cells with spring-loaded titanium pistons as a three-electrode system were used for electrochemical testing as described in Ref. [38]. After drying all cell parts at 120 °C, the cells were assembled inside an Ar-filled glovebox. When using sodium metal, great importance was paid to the preparation of the counter and reference electrodes as proposed in Ref. [13]. The surface was removed thoroughly with particular care to obtain a smooth surface to avoid inhomogeneity and impurities. The counter electrodes were pressed to a uniform thickness of 1 mm. It is crucial to compare the Na half-cells with another half-cell setup where one can exclude the effect of cathode decomposition as in full-cells. We used two different half-cell setups to characterize the LTO working electrodes: i) a sodium metal reference electrode and a 12 mm diameter sodium disc as counter electrode and ii) AC as the QRE and a 12 mm diameter AC disc as counter electrode. The cells are referred to as L/Na (i) and L/AC (ii). In both cases, the counter electrode and the LTO working electrodes were separated by a 13 mm diameter vacuum-dried glass-fiber disc (Whatman GF/D). Cells that were cycled for XPS analysis were additionally separated by a cellulose separator (Nippon Kodoshi). This separator was placed on top of the LTO electrode to avoid the adhesion of glass fibers on the surface. An aluminum foil current collector was placed on the backside of each counter electrode. The Na reference electrode and the QRE were placed on a compressed glass fiber separator (GF/D, from Whatman) in a cavity close to the working electrode/counter electrode stack and contacted with a titanium wire. The cells were vacuum filled with three different electrolytes, using the same electrolytes for a L/AC and L/Na cell, respectively.

Electrochemical measurements were carried out in a climate chamber at 25 °C by using a VMP3 multi-channel potentiostat/galvanostat (Bio-logic Science Instrument, France), equipped with the EC-Lab software. Galvanostatic charge/discharge cycling with potential limitation (GCPL) experiments were performed in voltage windows of 0.1–2.2 V (vs. Na/Na$^+$) and −2.5–0.4 V (vs. carbon) with a charge/discharge current of 50 mA g^{-1}. The cycling stability measurements were stopped after 100 cycles. Cells that were prepared for XPS analysis were stopped after 20 cycles in the sodiated state. All capacity values stated in this work are given with respect to the active material mass.

X-ray diffraction measurements

Ex situ X-ray diffraction (XRD) measurements of cycled electrodes were performed with a STOE STADI P diffractometer (CuK$_{\alpha 1}$-radiation, $\lambda = 1.5406$ Å) in flat-sample transmission mode. For phase identification, the ICSD database was utilized.

L/Na and L/AC cells, soaked in E-NaClO$_4$, were polarized to 2.2 V (vs. Na/Na$^+$) after 100 cycles. The potential was held for 2 h to obtain full desodiation. Afterwards, the cells were disassembled in air and the electrodes were washed with DMC to remove the remaining salt. The electrode coating was carefully removed from the aluminium foil of the cycled cells electrodes and from a pristine electrode. The obtained electrodes without current collector were characterized by XRD.

XPS analysis

L/AC and L/Na cells filled with E-NaClO$_4$, P-NaClO$_4$, and E-NaPF$_6$ were charged/discharged 20 times and stopped in the sodiated state at 0.1 V (vs. Na/Na$^+$) and −2.5 V (vs. carbon). The cells were transferred to an Ar-filled glovebox for disassembly. The LTO electrodes were then removed and rinsed with DMC prior to XPS measurements. The electrodes were transferred to the XPS measurement chamber in an inert atmosphere to minimize the surface reactions and contaminations from air. X-ray photoemission measurements were performed by using a K-Alpha XP spectrometer from Thermo Fisher Scientific (East Grinstead, UK). The samples were illuminated with monochromatic AlK$_\alpha$ X-rays with a spot size of analysis of 400 μm. The photoelectrons were detected with a hemispherical 180 dual focus analyzer with 128 channel detectors.

Conflict of interest

The authors declare no conflict of interest.

[1] D. Kundu, E. Talaie, V. Duffort, L. F. Nazar, Angew. Chem. Int. Ed. 2015, 54, 3431–3448; Angew. Chem. 2015, 127, 3495–3513.
[2] D. Larcher, J.-M. Tarascon, Nat. Chem. 2015, 7, 19–29.
[3] J.-M. Tarascon, Nat. Chem. 2010, 2, 510.
[4] a) V. Palomares, P. Serras, I. Villaluenga, K. B. Hueso, J. Carretero-González, T. Rojo, Energy Environ. Sci. 2012, 5, 5884–5901; b) J. Barker, M. Y. Saidi, J. L. Swoyer, Electrochem. Solid-State Lett. 2003, 6, A1–A4; c) P. Senguttuvan, G. Rousse, V. Seznec, J.-M. Tarascon, M. R. Palacín, Chem. Mater. 2011, 23, 4109–4111.
[5] A. Ponrouch, E. Marchante, M. Courty, J.-M. Tarascon, M. R. Palacín, Energy Environ. Sci. 2012, 5, 8572–8583.
[6] a) M. Dahbi, N. Yabuuchi, K. Kubota, K. Tokiwa, S. Komaba, Phys. Chem. Chem. Phys. 2014, 16, 15007–15028; b) J. Ajuria, E. Redondo, M. Arnaiz, R. Mysyk, T. Rojo, E. Goikolea, J. Power Sources 2017, 359, 17–26.
[7] C. Bommier, X. Ji, Small 2018, 14, 1703576.
[8] S. Fleischmann, M. Widmaier, A. Schreiber, H. Shim, F. M. Stiemke, T. J. S. Schubert, V. Presser, Energy Storage Mater. 2019, 16, 391–399.
[9] G. Hasegawa, K. Kanamori, T. Kiyomura, H. Kurata, K. Nakanishi, T. Abe, Adv. Energy Mater. 2015, 5, 1400730.
[10] W. Sun, X. Rui, J. Zhu, L. Yu, Y. Zhang, Z. Xu, S. Madhavi, Q. Yan, J. Power Sources 2015, 274, 755–761.
[11] D. I. Iermakova, R. Dugas, M. R. Palacín, A. Ponrouch, J. Electrochem. Soc. 2015, 162, A7060–A7066.
[12] M. Zarrabeitia, M. Muñoz-Márquez, F. Nobili, T. Rojo, M. Casas-Cabanas, Batteries 2017, 3, 16.
[13] J. Conder, C. Villevieille, Chem. Commun. 2019, 55, 1275–1278.
[14] a) P. W. Ruch, D. Cericola, M. Hahn, R. Kötz, A. Wokaun, J. Electroanal. Chem. 2009, 636, 128–131; b) M. Widmaier, B. Krüner, N. Jäckel, M. Aslan, S. Fleischmann, C. Engel, V. Presser, J. Electrochem. Soc. 2016, 163, A2956–A2964; c) M. Arnaiz, J. L. Gómez-Cámer, J. Ajuria, F. Bonilla, B. Acebedo, M. Jáuregui, E. Goikolea, M. Galceran, T. Rojo, Chem. Mater. 2018, 30, 8155–8163; d) D. Weingarth, A. Foelske-Schmitz, A. Wokaun, R. Kötz, Electrochem. Commun. 2012, 18, 116–118; e) J. Lee, N. Jäckel, D. Kim, M. Widmaier, S. Sathyamoorthi, P. Srimuk, C. Kim, S. Fleischmann, M. Zeiger, V. Presser, Electrochim. Acta 2016, 222, 1800–1805; f) S.

Fleischmann, K. Pfeifer, M. Widmaier, H. Shim, Ö. Budak, V. Presser, *ACS Appl. Energy Mater.* **2019**, *2*, 3633–3641.

[15] N. Mozhzhukhina, E. J. Calvo, *J. Electrochem. Soc.* **2017**, *164*, A2295–A2297.

[16] D. Stępień, Z. Zhao, S. Dsoke, *J. Electrochem. Soc.* **2018**, *165*, A2807–A2814.

[17] Z. Ding, V. Trouillet, S. Dsoke, *J. Electrochem. Soc.* **2019**, *166*, A1004–A1014.

[18] a) R. Alcántara, P. Lavela, G. F. Ortiz, J. L. Tirado, *Electrochem. Solid-State Lett.* **2005**, *8*, A222–A225; b) D. Hamani, M. Ati, J.-M. Tarascon, P. Rozier, *Electrochem. Commun.* **2011**, *13*, 938–941; c) P. Vassilaras, X. Ma, X. Li, G. Ceder, *J. Electrochem. Soc.* **2013**, *160*, A207–A211.

[19] Y. Sun, L. Zhao, H. Pan, X. Lu, L. Gu, Y.-S. Hu, H. Li, M. Armand, Y. Ikuhara, L. Chen, X. Huang, *Nat. Commun.* **2013**, *4*, 1870.

[20] a) A. J. Bard, L. R. Faulkner, *Fundamentals and Applications*, Wiley, New York, **2001**; b) C. M. A. Brett, A. M. O. Brett, *Principles, methods and applications*, Oxford University Press, Oxford, **1993**.

[21] a) S. Klink, E. Madej, E. Ventosa, A. Lindner, W. Schuhmann, F. La Mantia, *Electrochem. Commun.* **2012**, *22*, 120–123; b) J. Song, *J. Power Sources* **2002**, *111*, 255–267.

[22] D. A. Stevens, J. R. Dahn, *J. Electrochem. Soc.* **2000**, *147*, 1271–1273.

[23] D. A. Stevens, J. R. Dahn, *J. Electrochem. Soc.* **2001**, *148*, A803–A811.

[24] M. Widmaier, N. Jäckel, M. Zeiger, M. Abuzarli, C. Engel, L. Bommer, V. Presser, *Electrochim. Acta* **2017**, *247*, 1006–1018.

[25] X. Yu, H. Pan, W. Wan, C. Ma, J. Bai, Q. Meng, S. N. Ehrlich, Y.-S. Hu, X.-Q. Yang, *Nano Lett.* **2013**, *13*, 4721–4727.

[26] F. Zhao, P. Xue, H. Ge, L. Li, B. Wang, *J. Electrochem. Soc.* **2016**, *163*, A690–A695.

[27] L. Y. Yang, H. Z. Li, J. Liu, S. S. Tang, Y. K. Lu, S. T. Li, J. Min, N. Yan, M. Lei, *J. Mater. Chem. A* **2015**, *3*, 24446–24452.

[28] a) A. J. Smith, J. C. Burns, S. Trussler, J. R. Dahn, *J. Electrochem. Soc.* **2010**, *157*, A196–A202; b) B. Gyenes, D. A. Stevens, V. L. Chevrier, J. R.

Dahn, *J. Electrochem. Soc.* **2015**, *162*, A278–A283; c) S. Komaba, T. Ishikawa, N. Yabuuchi, W. Murata, A. Ito, Y. Ohsawa, *ACS Appl. Mater. Interfaces* **2011**, *3*, 4165–4168; d) J. Wang, Y. Bai, M. Wu, J. Yin, W. F. Zhang, *J. Power Sources* **2009**, *191*, 614–618.

[29] a) W. Shen, Z. Li, Y. Liu, *CHENG* **2008**, *1*, 27–40; b) Y. Zhang, X. Li, J. Huang, W. Xing, Z. Yan, *Nanoscale Res. Lett.* **2016**, *11*, 163.

[30] M. Widmaier, K. Pfeifer, L. Bommer, V. Presser, *Batteries Supercaps* **2018**, *1*, 11–26.

[31] S. Ghosh, S. Mitra, P. Barpanda, *Electrochim. Acta* **2016**, *222*, 898–903.

[32] B. Philippe, M. Valvo, F. Lindgren, H. Rensmo, K. Edström, *Chem. Mater.* **2014**, *26*, 5028–5041.

[33] S. Komaba, W. Murata, T. Ishikawa, N. Yabuuchi, T. Ozeki, T. Nakayama, A. Ogata, K. Gotoh, K. Fujiwara, *Adv. Funct. Mater.* **2011**, *21*, 3859–3867.

[34] T. Sultana, G. L. Georgiev, G. Auner, G. Newaz, H. J. Herfurth, R. Patwa, *Appl. Surf. Sci.* **2008**, *255*, 2569–2573.

[35] L. Bodenes, A. Darwiche, L. Monconduit, H. Martinez, *J. Power Sources* **2015**, *273*, 14–24.

[36] M. Dahbi, T. Nakano, N. Yabuuchi, T. Ishikawa, K. Kubota, M. Fukunishi, S. Shibahara, J.-Y. Son, Y.-T. Cui, H. Oji, S. Komaba, *Electrochem. Commun.* **2014**, *44*, 66–69.

[37] A. Ponrouch, R. Dedryvère, D. Monti, A. E. Demet, J. M. A. Mba, L. Croguennec, C. Masquelier, P. Johansson, M. R. Palacín, *Energy Environ. Sci.* **2013**, *6*, 2361–2369.

[38] D. Weingarth, M. Zeiger, N. Jäckel, M. Aslan, G. Feng, V. Presser, *Adv. Energy Mater.* **2014**, *4*, 1400316.